Prabin Kumar Mahato [1]*, *Swarat Choudhuri* [2], *Shristi Chaudhary*[3], *Prashanta Patra*[4], *Deepak Gupta*[5]

1Department of Physics, Ranchi University, Ranchi, 834008, India
2Department of Physics, St. Xavier College, Ranchi, 834001, India
3Department of Physics, Chandigarh University, Gharuan, Mohali, Punjab, 140413, India, 4Department of Physics, Kolhan University, Chaibasa, 833202, India, 5School of Basic and Applied Sciences, Galgotias University, Greater Noida, 203201, India

Scientific paper
ISSN 0351-9465, E-ISSN 2466-2585
https://doi.org/10.62638/ZasMat1069

Zastita Materijala 66 ( )
(2025)

Morphological, size-dependent field emission investigation of GO and rGO nanosheet

ABSTRACT

Here, we report the role of surface morphologies and grain size on the electron field emission characteristics of GO and rGO nanosheets, synthesized through a modified Hummer's method. Plasmon peaks were observed at 290 nm to 310 nm for both samples. A plasmonic energy-associated effective mass model was used to calculate the crystal size of the nanosheets, which was found to be 3.56 nm and 4.79 nm for GO and rGO, respectively, confirming confinement behavior. Raman spectroscopy data recorded for GO and rGO nanosheets confirmed the presence of D and G bands, indicating the successful growth of both GO and rGO. Additionally, the crystal size calculated from the Raman data is comparable to the Bohr exciton radius, suggesting that GO and rGO exhibit quantum dot-like behavior. The electron field emission parameters of the synthesized GO and rGO nanosheets were investigated, and the parameters were calculated using the Fowler–Nordheim (F-N) equation. Among the samples, the GO nanosheets exhibited the best electron field emission properties, with a minimum turn-on voltage of 8.2 V/μm and a field enhancement factor of 1200, attributed to the smallest emitter tip radius and the varying surface morphologies.

Keywords: *Graphene oxide, Raman Density, compression, porous, thermal Field Emission conductivity*

1. INTRODUCTION

Graphene and its derivatives, such as graphene oxide (GO) and reduced graphene oxide (rGO) are said to be effective and promising materials for many applications. Graphene shows a 2D structure, where a uniform, homogeneous single layer of carbon (Z=6) atoms are set in a hexagonal lattice plane and play a significant role in emission properties [1]. Moreover, graphene and its derivatives (GO and rGO) are usually flat with better transmission and efficient charge transfer [2]. Since graphene is getting attraction in nano and tech. fields. Graphene shows high surface area, a variable energy gap, extraordinary thermal as well as electrical conductivity, and excellent mobility at room temperature [3]. The GO is a carbon layer with the presence of oxygen functional, that is attached to both sides of the carbon layer and the carbon edges of the plane [4].

GO could be a single or multilayer sheet. A 2-dimensional sheet with a single layer is GO; two double layers of GO are named two-layered GO [5]. Moreover, the 2-dimensional GO layer in between two to five layers is called a few-layered GO sheet, and more than five layers are said to be multilayer GO [6]. GO nanosheets are synthesized by the modified Hummer method [7] that controls the morphology and size of nanostructure, which play an important role in electron field emission properties [8].

Electron field emission is the important characteristic of electron emission by the emitter surface height barrier of a structure through the principle of quantum tunnel phenomenon [9]. In the basic theory of thermionic emission (TE), the emitter (GO and rGO) are annealed at extreme temperatures to transfer enough energy to excited electrons, which is needed to discuss the work function of the emitter of the nanosheet [10]. While, the electron field emission is produced under the most intense external applied electric field to an

*Corresponding author: Prabin Kumar Mahato
E-mail: pkmahatoru@gmail.com
Paper received: 12. 04 2024.
Paper accepted: 28. 09. 2024.
the website: https://www.zastita-materijala.org/

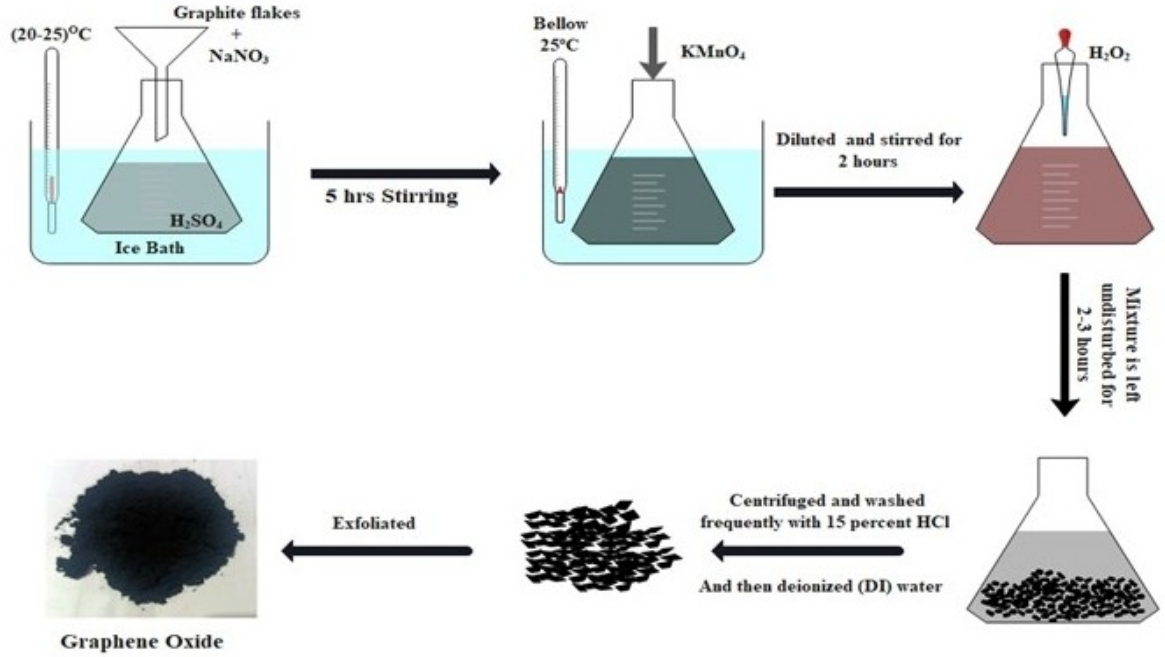

Figure1: *Schematic diagram of synthesis of GO.*

emitter surface (as cathode), called cold cathode emission [12]. These electron emissions are used for various applications including microwave generation devices, gas sensors, field emission displays, and medical imaging [13]. Various groups made an effort to investigate the field emission properties of different nanostructures [9,14,15]. The majority of previously reported investigations on electron field emission of graphene, GO and rGO nanosheets have not focused in detail. However, the correlation between morphologies and grain size (calculated from the EMA model) with electron field emission properties has been rarely reported yet. This investigation reports the role of morphology and grain size on the performance of electron field emission of GO and rGO. The theoretical effective mass models are used to calculate the size using different absorption plasmonic energy. A correlation between morphologies and grain size and electron field emission properties exhibits that the turn-on field is effectively impacted by the size quantum effect in GO and rGO nanosheets.

2. MATERIALS AND METHODS

Graphene oxide (GO) is synthesized through the improved Hummers' method. In the Hummers' method, graphite is oxidized using a mixture of concentrated sulfuric acid (H_2SO_4), sodium nitrate ($NaNO_3$), and potassium permanganate ($KMnO_4$). H_2O_2 is used to stop the reaction. The resultant solution is centrifuged using HCl, and dried in the presence of IR at 85°. Finally, GO is obtained by exfoliating using heat treatment. The oxidation process introduces oxygen-containing functional groups such as hydroxyl (-OH), epoxide (-O-), and carboxyl (-COOH) onto the graphene layers, resulting in the formation of GO. After obtaining GO, reduced graphene oxide (rGO) is prepared by reducing the oxygen-containing functional groups in GO using sodium Borohydride[16-17]. The reduction process removes some of the oxygen groups and partially restores the sp2 carbon network, leading to the formation of rGO. The schematic of synthesis process is shown in Fig 1.

3. RESULTS AND DISCUSSION

3.1 Morphological and elemental composition of GO and rGO.

Fig. 2(a-b) displays the FESEM micrograph of graphene oxide (GO) and reduced graphene oxide (rGO) samples. Fig. 2(a) shows the presence of crumple and spherical type structure, because of the exfoliation of graphite sheet, which becomes to GO nanosheet and results in reduction or deformation on the exfoliation. Fig. 2(b) displays the micrograph of reduced graphene oxide (rGO), the folded and wrinkled nanostructure has been found. This folding rGO nanosheet is observed on the surface and the edge of rGO due to the losses of the presence of oxygen functional groups[18]. More folded and wrinkled nanosheet is produced when the reduction is quite stronger. A layered sheet with few defects is found in both samples, indicating their polycrystalline behavior. Relatively, the rGO nanosheet shows more aggregation than

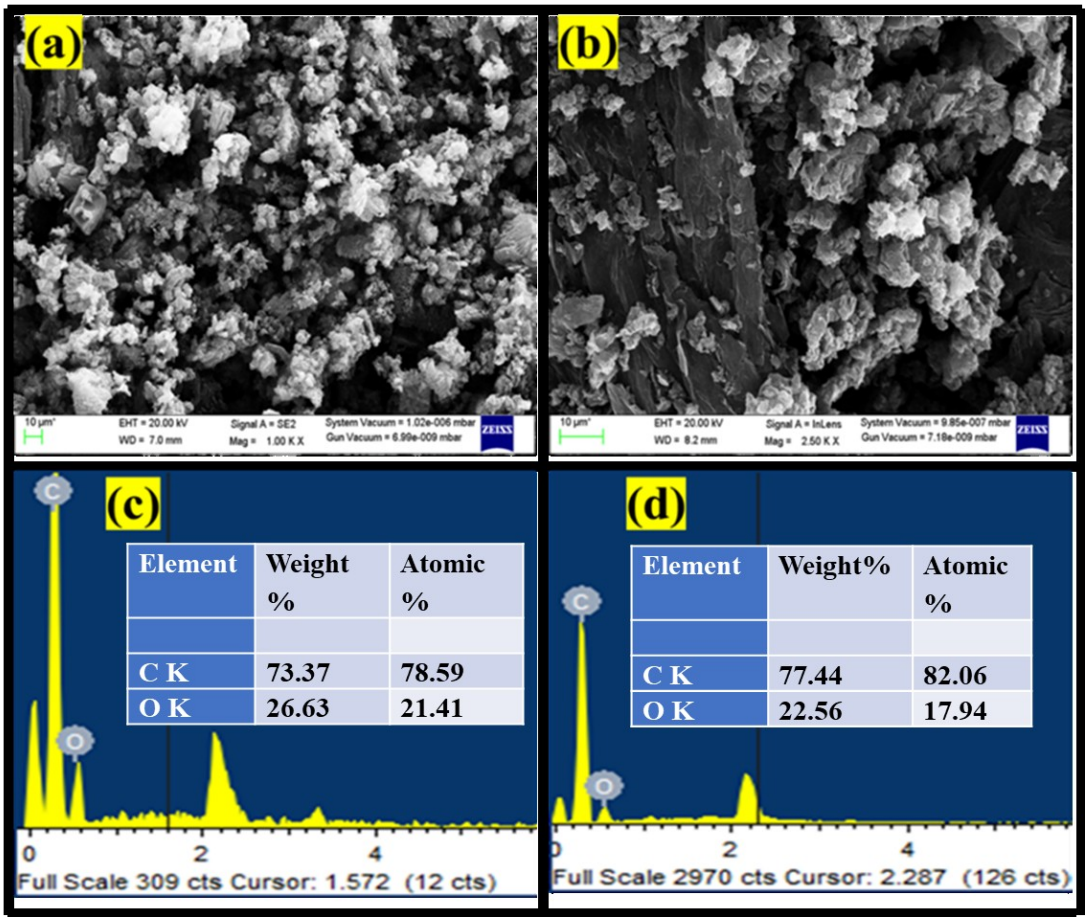

***Figure 2**: FESEM and EDS spectra, (a-c) GO, (b-d) rGO.*

the GO. The ratio of C:O for GO and rGO nanosheets has been investigated through EDS measurement, as shown in Fig.2(c-d). The ratios of C:O of GO and rGO are 1.48 and 2.53, respectively. The EDS result confirms the reduction of rGO from the GO nanosheet [19].

3.2 XRD study of GO and rGO

XRD spectra were recorded by using Cu (Kα) radiation (0.154 nm) and intensity was collected in range of 2θ = 5–40◦ for GO and rGO nanosheet to evaluate the structural and elastic properties, as shown in Fig. 3. The observed peaks corresponding to reflection planes (001) at 2θ = 11.8◦ assigned to GO phase and observed peaks corresponding to reflection planes (002) at 2θ = 26.8◦ assigned to rGO phase [JCPDS card no. 77-2306] . The structural parameters such as crystal size (D), lattice strain (ε), and dislocation density (δ) have been studied corresponding to (001) and (002) reflection peak of GO and rGO nanosheet are estimated using the Scherer equation [20].

$$D = \frac{k\lambda}{\beta_D \cos\theta} \qquad \text{.....(1)}$$

$$\varepsilon = \frac{\beta_{hkl}}{4\tan\theta} \qquad \text{.....(2)}$$

Here β_D is full-width at half maximum (FWHM). The estimated average values of D of GO and rGO nanosheet using Scherrer's formula are 2.9 nm and 6.6 nm. The analysis of disorderness, non-uniformity, non-homogeneity, irregularities and crystal defects present in samples has been carried out using dislocation density (δ), calculated through following equation [21]:

$$\delta = \left(\frac{\beta_D \cos\theta}{k\lambda}\right)^2 = \frac{1}{D^2} \qquad \text{.....(3)}$$

The estimated average value of dislocation density of GO and rGO nanosheet are 0.1228 and 0.0229 respectively.

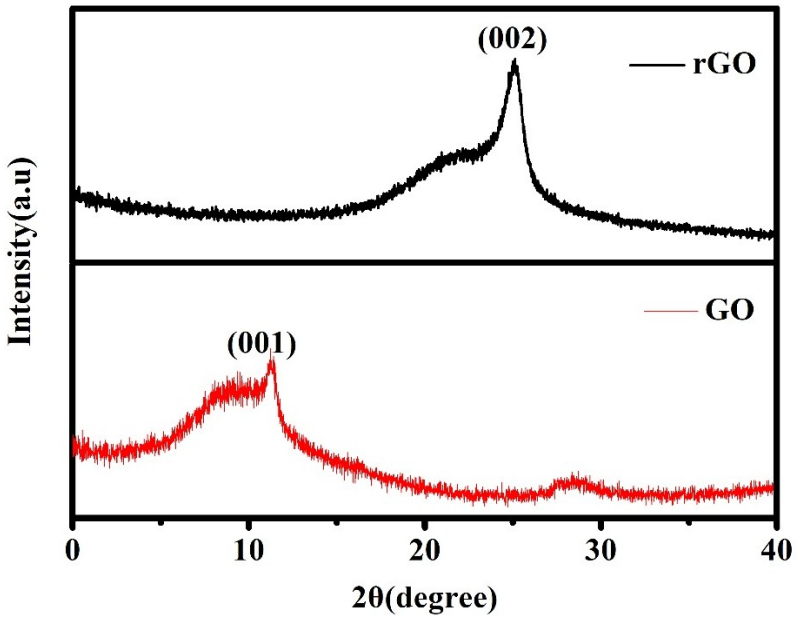

Figure 3: *XRD of GO and rGO nanoseet*

3.3 Optical and Raman study of GO and rGO

The optical absorption properties of the GO and rGO are shown in Fig. 4(a), The GO exhibits the peak position at 290 nm indicating the p–n* absorption band, on the other hand, the rGO exhibits the peak position at 298 nm indicate the p–n* absorption band, suggest that some groups on the GO nanosheet are eliminated and the conjugated nanostructures have been restored. The surface plasmonic position centered at 230 nm for the GO nanosheet is red-shifted (shifting towards a higher wavelength) with increasing reduction i.e GO to rGO samples. Further, red shifting can be explained through the quantum confinement effect through various theoretical models using optical absorption. Here we will use the effective mass model to compute the size, which is expressed as [22-24].

$$E_g^* = E_g^{bulk} - \frac{1.8e^2}{4\pi\varepsilon_0\varepsilon_r} + \frac{\hbar^2\pi^2}{2r^2}\left(\frac{1}{m_e^*} + \frac{1}{m_h^*}\right) \quad ..(4)$$

Where r is the crystallite radius. The calculated size from this model are 3.56 nm and 4.79 nm respectively for both the samples. Besides the effective mass model, another model called the Hyperbolic Band approximation (HBA) model, is used to estimate the size of GO and rGO. The HBA model is expressed as [25-26].

$$E_g^2 = E_g^{bulk} + \left(\frac{2\hbar^2 E_{bulk}}{\mu}\right)\left(\frac{\pi}{r}\right)^2 \quad \text{.....(5)}$$

The estimated crystallite size from this model is 8.45nm and 11.76nm.

Raman spectroscopy is used to investigate the defects and disorders present in synthesized samples of GO and rGO. Fig.4(b) displays the Raman spectra for both samples, which exhibit two significant bands namely the G band and D band. In the recorded GO and rGO samples, the G band centered at ~ 1540-1545 cm^{-1}, indcates the perfect GO and rGO nanostructure of a carbon atom with sp^2 hybridization mode and is assigned to E2g-symmetry phonons. The D band is centered at 1350-1380 cm^{-1}, indicating the A1g-symmetry phonons and which confirm the presence of defects in samples. The defect(D) band suggests the disorder in samples arises because of microstructural imperfections and irregularities by the presence of functional groups in the 2-dimensional. graphene sheets. The G-band comes in our samples because of lattice plane vibration of sp^2 hybridized mode of carbon atoms. In the case of the GO nanosheet, the functional groups are fond of the carbon atoms by shifting the hybridization mode from sp2 to sp3 mode. On the other hand, the rGO shows the red shifting of the G band than the GO nanosheet. The Raman intensity ratio of D-band (I_D) and G-band (I_G) is also estimated, which gives the information of qualitative assessment of the presence of disorder, defects in the GO and rGO samples. The I_D/I_G ratio decreases from 0.81 to 0.92 for the samples. The I_D/I_G ratio of Raman band decreases with the reduction of graphene oxide. To estimate the grain size from recorded Raman spectra through expression [27], $L_a = \frac{560}{E^4}\left(\frac{I_D}{I_G}\right)^{-1}$, where E is laser energy

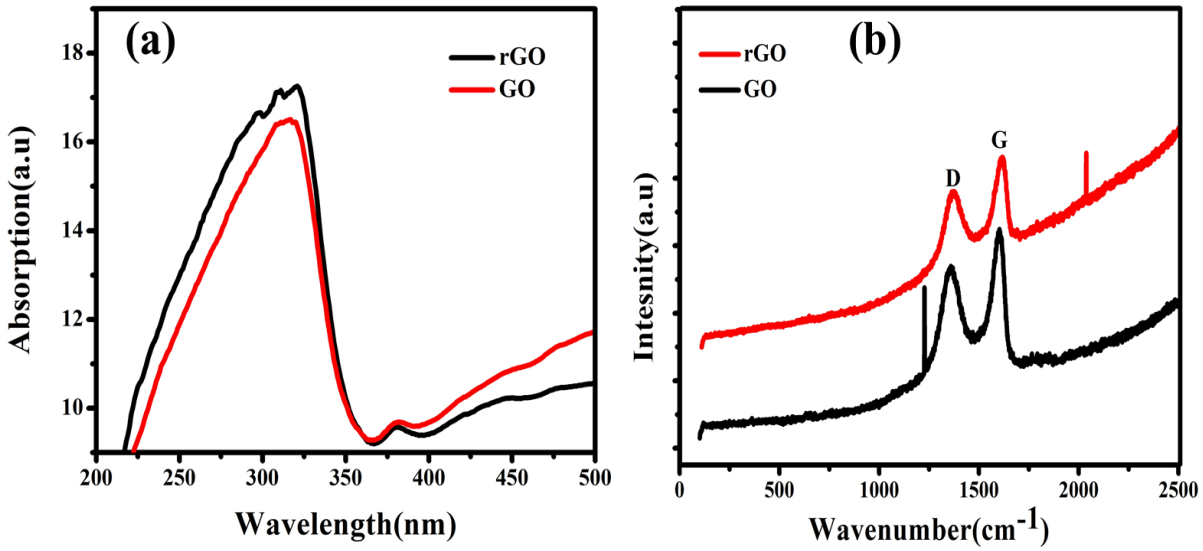

Figure 4: *(a) absorption, (b) Raman spectra of GO and rGO.*

and expression $L_a = 2.4\times10^{-10}\lambda^4\left(\frac{I_D}{I_G}\right)^{-1}$,is used to calculate the size. The estimated Size was 17 and 23 nm for GO and rGO.

3.4 Field emission properties of GO and rGO

Graphene and its derivatives show promising electron field emission behavior and are examined for application in devices. To understand the emission properties of nanosheets, the electron emissions testing is carried out with diode assembly inside the chamber at a minimum pressure, and the separation between the cathode and anode was 0.025cm. A schematic diagram of field emission geometry is shown in Fig. 5. The process of field emission depends on the principle of quantum tunneling phenomenon. Fig. 6(a-b) displays the current density (J) versus applied electric field(E) curve plots for both samples. The turn-on voltage for collection of GO is usually expressed as the electric field needed to create the emission current densities of 15 mA-cm^{-2}. The turn on voltage values is found to be 8.67 V/μm and 9.2 V/μm for both the samples. A morphology and size dependent on turn on voltage, indicate that turn-on fields are possibly tailored through tailoring the GO and rGO diameter. A minimum turn on voltage is required for electron field emission from synthesized GO and rGO samples are used for minimal power operation-based devices. It is evidence that the emission behavior of nanosheet is effectively impacted with size. It is required to turn on voltage of GO and rGO shows minimum size because of larger applied external field at the tip of the nanosheet.

The electron field emission data have been investigated through the Fowler–Nordheim (FN) model which tells about the electron emission current density through barrier tunneling phenomenon, electron field emission current as a function of the applied external electric field and are expressed as follows [28-29].

$$J = \frac{K\beta^2 v^2}{\phi}\exp\left(-\frac{PW^{3/2}}{\beta V}\right) \quad \text{.....(6)}$$

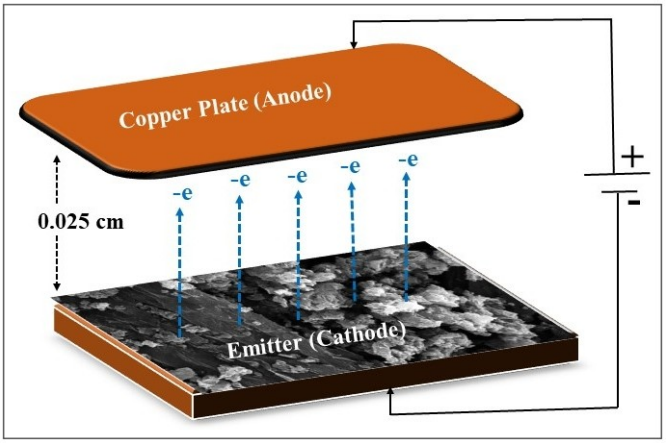

Figure 5: *Schematic diagram of field emission geometry.*

where K (= 1.541 × 10^{-6} AV^{-2} eV) is a constant, P = 6831 eV$^{-3/2}$ μm^{-1} V, V is the applied electric field, φ is the work function and β is the field-enhancement factor. The plot of ln(J/E^2) with (1/E) is defined as FN plot, whose gradient is expressed as.

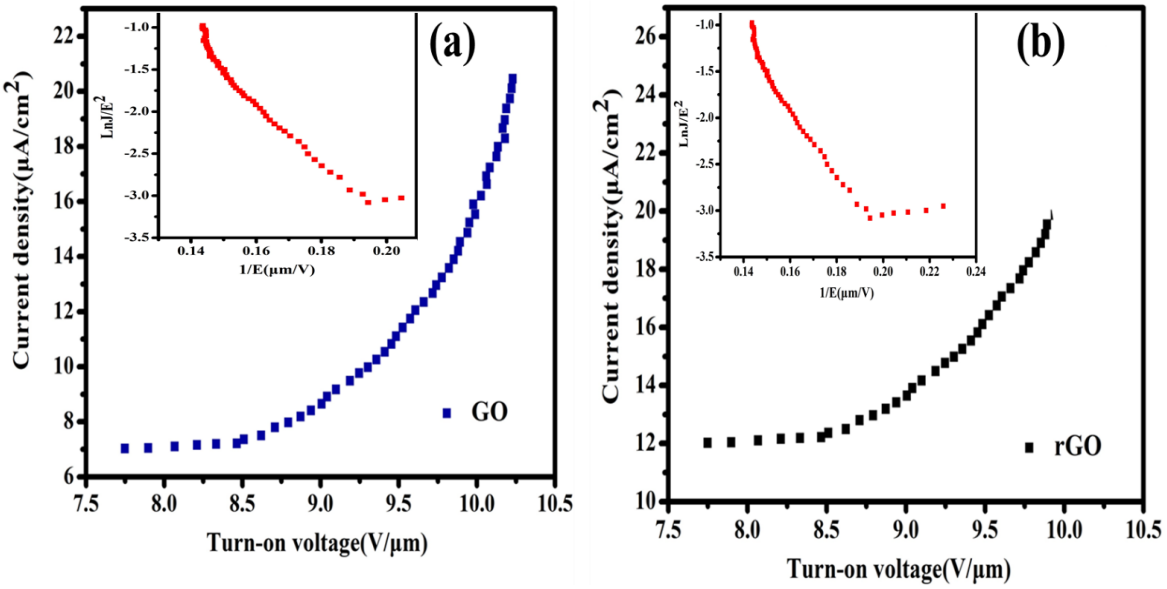

Figure 6: *Electron emission current–voltage plot (inset FN plot) of (a) GO, (b) rGO nanosheet.*

4. CONCLUSIONS

This investigation demonstrated the synthetization of GO and rGO through a modified hummer method. XRD pattern confirm the formation of GO and rGO phase. The plasmon peaks were observed at 290 nm to 310 nm for both the samples. Here, a plasmonic energy associated effective mass model was used to calculate the crystal size of nanosheet, which is 3.56 nm and 4.79 nm for GO and rGO nanosheet, which confirm the confinement behavior. The G band is centered at ~1540-1545 cm^{-1}, and the D band is centered at 1350 to 1380 cm^{-1}, indicating the A1g-symmetry phonons and which confirm the presence of defects in samples. An excellent field emission for GO was found with minimum turn-on voltage of 6 V/μm. The synthesized GO has proved to be an excellent electron field emitter. On the other hand, the field enhancement factors are 1200 and 1160 for both samples. A maximum field enhancement factor was found for a smaller crystal size sample. A size dependent change in turn-on field suggests that electron field emission parameters are also be tailored as a result of size confinement in GO and rGO nanosheets.

5. REFERENCES

[1] T. M. Magne, et. Al., (2022) Graphene and its derivatives: understanding the main chemical and medicinal chemistry roles for biomedical applications. Journal of nanostructure in chemistry, 12, 693-727. *https://doi.org/10.1007/s40097-021-00444-3*

[2] R. S. Krishna, J. Mishra, B. Nanda, S. K. Patro, A. Adetayo, T. S. Qureshi (2021) The role of graphene and its derivatives in modifying different phases of geopolymer composites: A review. Construction and Building Materials, 306, 124774. *https://doi.org/10.1016/j.conbuildmat.2021.124774*

[3] V. B. Mbayachi, E. Ndayiragije, T. Sammani, S. Taj, E. R. Mbuta (2021) Graphene synthesis, characterization and its applications: A review. Results in Chemistry, 3, 100163. *https://doi.org/10.1016/j.rechem.2021.100163*

[4] J. Liu, S. Chen, Y. Liu, B. Zhao (2022) Progress in preparation, characterization, surface functional modification of graphene oxide: A review. Journal of Saudi Chemical Society, 26(6), 101560. *https://doi.org/10.1016/j.jscs.2022.101560*

[5] T. R. Mignoli, T. L. Hewer, R. A. Antunes, R. M. Alves, M. Schmal (2021) Synthesis of few-layered graphene sheets as support of cobalt nanoparticles and its influence on CO hydrogenation. Materials Science and Engineering: B, 273, 115388. *https://doi.org/10.1016/j.mseb.2021.115388*

[6] Y. Cao (2024) Rhombohedral graphene goes correlated at four or five layers. Nature Nanotechnology, 19(2), 139-140. *https://doi.org/10.1038/s41565-023-01566-1*

[7] N. I. Zaaba, K. L. Foo, U. Hashim, S. J. Tan, W. W. Liu, C. H. Voon (2017) Synthesis of graphene oxide using modified hummers method: solvent influence. Procedia engineering, 184, 469-477. *https://doi.org/10.1016/j.proeng.2017.04.118*

[8] S. Santandrea, F. Giubileo, V. Grossi, S. Santucci, M. Passacantando, T. Schroeder, ... A. Di Bartolomeo (2011) Field emission from single and few-layer graphene flakes. Applied Physics Letters, 98(16). *https://doi.org/10.1063/1.3579533*

[9] V. Kashyap, C. Kumar, N. Chaudhary, K. Saxena (2022) The role of quantum crystal radius on electron field emission properties of fractal silicon nanowire arrays. Materials Letters, 314, 131842. *https://doi.org/10.1016/j.matlet.2022.131842*

[10] I. Lahiri, V. P. Verma, W. Choi (2011) An all-graphene based transparent and flexible field emission device. Carbon, 49(5), 1614-1619. *https://doi.org/10.1016/j.carbon.2010.12.044*

[11] C. Kumar, V. Kashyap, A. Kumar, A. K. Sharma, D. Gupta, D. P. Singh, K. Saxena (2023) Reframe of Fowler-Northeim Approach for Electron Field Emission of a Vertical Silicon Nanowires. Silicon, 15(15), 6591-6602. *https://doi.org/10.1007/s12633-023-02505-4*

[12] V. Kashyap, C. Kumar, N. Chaudhary, K. Saxena (2023) Quantification of deviation of size dependent field enhancement factor of silicon nanowires array through theoretical modeling. Silicon, 15(3), 1203-1210. *https://doi.org/10.1007/s12633-022-02068-w*

[13] S. Nirantar, T. Ahmed, M. Bhaskaran, J. W. Han, S. Walia, S. Sriram (2019) Electron emission devices for energy-efficient systems. Advanced Intelligent Systems, 1(4), 1900039. *https://doi.org/10.1002/aisy.201900039*

[14] Y. W. Zhu, et.al., (2003) Efficient field emission from ZnO nanoneedle arrays. Applied Physics Letters, 83(1), 144-146. *https://doi.org/10.1063/1.1589166*

[15] L. Chen, H. Yu, J. Zhong, J. Wu, W. Su (2018) Graphene based hybrid/composite for electron field emission: a review. Journal of Alloys and Compounds, 749, 60-84. *https://doi.org/10.1016/j.jallcom.2018.03.100*

[16] S. N. Alam, N. Sharma, L. Kumar (2017) Synthesis of graphene oxide (GO) by modified hummers method and its thermal reduction to obtain reduced graphene oxide (rGO). Graphene, 6(1), 1-18. *http://dx.doi.org/10.4236/graphene.2017.61001*

[17] T. K. Kuanyshbekov, K. Akatan, S. K. Kabdrakhmanova, R. Nemkaeva, M. Aitzhanov, A. Imasheva, E. Kairatuly (2021) SYNTHESIS OF GRAPHENE OXIDE FROM GRAPHITE BY THE HUMMERS METHOD. Oxidation Communications, 44(2).

[18] N. Sharma, V. Sharma, Y. Jain, M. Kumari, R. Gupta, S. K. Sharma, K. Sachdev (2017) Synthesis and characterization of graphene oxide (GO) and reduced graphene oxide (rGO) for gas sensing application. In Macromolecular symposia. 376(1), 1700006. *https://doi.org/10.1002/masy.201700006*

[19] N. Aslan, B. Aksakal (2021) Effect of graphene reinforcement on hybrid bioceramic coating deposited on the produced porous Ti64 alloys. Journal of Porous Materials, 28(4), 1301-1313. *https://doi.org/10.1007/s10934-021-01081-5*

[20] C. Kumar, M. Shrivastav, J. Escrig, L. P. Campos, A. I. Martinez, H. Silva, A. Zarate (2024) The investigation of thickness-dependent mono-fractal, optical and optoelectronics properties of sputtered silver thin film for silicon solar cell. Vacuum, 225, 113247. *https://doi.org/10.1016/j.vacuum.2024.113247*

[21] V. Kashyap, H. Pawar, I. Sihmar, C. Kumar, A. Kumar, S. Kumar, ... K. Saxena (2024) X-ray analysis of Ag nanoparticles on Si wafer and influence of Ag nanoparticles on Si nanowire-based gas sensor. Applied Physics A, 130(4), 238. *https://doi.org/10.1007/s00339-024-07379-w*

[22] V. Kashyap, C. Kumar, N. Chaudhary, N. Goyal, K. Saxena (2021) The correlation of resistivity with the crystal size present in silicon nanowires through confinement-based models. Materials Letters, 301, 130312. *https://doi.org/10.1016/j.matlet.2021.130312*

[23] P. Patra, R. Kumar, C. Kumar, P. K. Mahato (2022) Ni-incorporated cadmium sulphide quantum dots for solar cell: an evolution to microstructural and linear-nonlinear optical properties. Journal of Crystal Growth, 583, 126542. *https://doi.org/10.1016/j.jcrysgro.2022.126542*

[24] S. Pathak, S. Chaudhary, M. Shrivastav, N. Kumar, S. Varshney, M. Kumar, ... C. Kumar (2024) The effects of air-annealing on the performance of optical-electrical assessment of sputtered CdS film towards the Ag/n-CdS/p-Si (100)/Al photodetectors. Optical Materials, 150, 115117. *https://doi.org/10.1016/j.optmat.2024.115117*

[25] C. Kumar, V. Kashyap, M. Shrivastav, F. Guzman, D. P. Singh, K. Saxena (2023) In-depth opto-electrical analysis of Ni: CdS film towards the performance as Ag/Ni:CdS/FTO Schottky diode. Optical Materials, 143, 114226. *https://doi.org/10.1016/j.optmat.2023.114226*

[26] P. Patra, R. Kumar, C. Kumar, K. Pandey, P. K. Mahato (2023) Exploration of impact of thermal condition on microstructural-optical-electrical properties of Ni doped CdS thin films. Materials Today: Proceedings. *https://doi.org/10.1016/j.matpr.2023.07.018*

[27] P. K. Mahato, S. Choudhuri, C. Kumar, S. Roy, P. Patra (2023) Evaluation of crystal size present in graphene oxide quantum dots using optical and Raman spectroscopy. Materials Today: Proceedings, 80, 668-673.

[28] V. Kashyap, C. Kumar, V. Kumar, N. Chaudhary, K. Saxena (2022) Induced quantum-Fano effect by Raman scattering and its correlation with field emission properties of silicon nanowires. Applied Physics A, 128(4), 312. *https://doi.org/10.1007/s00339-022-05415-1*

[29] C. Kumar, V. Kashyap, J. M. Shrivastav, V. Kumar, F. Guzman, K. Saxena (2024) The dopant (n-and p-type)-, band gap-, size-and stress-dependent field electron emission of silicon nanowires. Physical Chemistry Chemical Physics, 26(25), 17609-17621. *https://doi.org/10.1039/D4CP00825A*

MORFOLOŠKO ISTRAŽIVANJE EMISIJE GO I rGO NANOLISTA ZAVISNO OD VELIČINE

IZVOD

Ovde se izlaže o ulozi morfologije površine i veličine zrna na karakteristike emisije elektronskog polja GO i rGO nanolistova, sintetizovanih modifikovanom Hamerovom metodom. Plazmonski pikovi su primećeni na 290 nm -310 nm za oba uzorka . Ovde je korišćen model efekti vne mase povezan sa plazmonskom energijom za izračunavanje veličine kristala nanolista, koja je 3,56 nm i 4,79 nm za GO i rGO nanolist, što potvrđuje ponašanje zatvaranja. Ramanski podaci snimljeni za GO i rGO nanolist potvrđuju prisustvo D i G traka, što sugeriše rast GO i rGO. Pored toga, veličina kristala se izračunava Ramanovim podacima, koji je uporediv sa veličinom radijusa Borovog eksitona, što ukazuje na GO i rGO kao kvantne tačke. Parametri emisije elektronskog polja sintetizovanih GO i rGO nanolistova su istraženi i parametri su izračunati pomoću Fauler –Nordhajmove (F-N) jednačine. Među njima, GO uzorak pokazuje najbolja svojstva emisije elektronskog polja sa minimalnim naponom uključivanja od 8,2 V/mm i faktorom poboljšanja polja od 1200 zbog posedovanja najmanjeg radijusa (veličine) vrha emitera i različite morfologije površine.

Ključne reči: Grafen oksid, Raman, Pojasni razmak, Emisija polja.

Scientific paper
Paper received: 11.09.2024.
Paper corrected: 22.11. 2024.
Paper accepted: 30.11.2024.

naucni rad
rad primljen 11.9.2024.
rad korigovan 22.11.2024.
rad prihvacen 30.11.2024.

[1*]Prabin Kumar Mahato: https://orcid.org/0000-0001-6718-4893
[4]Prashanta Patra: https://orcid.org/0000-0002-2425-1037
[5]Deepak Gupta : https://orcid.org/0000-0002-4228-2523